AUTOMATIC PIPELINE FOR LIGHT-CURVES VARIABILITY ANALYSIS OF GEO OBJECTS

Tommaso Cardona[(1)], Patrick Seitzer[(2)], Fabrizio Piergentili[(3)], Fabio Santoni[(4)]

[(1)] DIMA, Sapienza - University of Rome, Via Eudossiana 18, Roma (Italy), tommaso.cardona@uniroma1.it
[(2)] Astronomy Dept., University of Michigan, 1085 S University Ave, Ann Arbor, MI (USA), pseitzer@umich.edu
[(3)] DIMA, Sapienza - University of Rome, Via Eudossiana 18, Roma (Italy), fabrizio.piergentili@uniroma1.it
[(4)] DIAEE, Sapienza - University of Rome, Via Eudossiana 18, Roma (Italy), fabio.santoni@uniroma1.it

ABSTRACT

Active satellites at Geostationary Earth Orbit (GEO) are typically attitude controlled. This control ceases in the case of loss of control, or when the satellite is moved to a graveyard orbit, and decommissioned. When one of these events occurs, how does the attitude change with time? In this paper, rapid changes in brightness are investigated as possible implication of rapid changes in attitude. The short-term brightness variability of uncontrolled objects at GEO is studied by taking observations while the telescope is tracking at the sidereal rate, and the target is trailed across the field of view (FOV). Analysis of intensity changes along the trail reveals the primary frequencies of the object's brightness variations on time scales of a second or less. These observations were performed by using:

- The University of Michigan's 0.6m Curtis-Schmidt telescope located at the Cerro Tololo InterAmerican Observatory (Chile) equipped with a thinned, backside illuminated CCD with 1.45 arc-seconds/pixel and a FOV of 1.6x1.6 deg.
- The 1.5m Cassini telescope in Loiano (Italy), operated by the INAF (National Institute for Astrophysics) Astronomical Observatory of Bologna, equipped with BFOSC (Bologna Faint Object Spectrograph and Camera), a multipurpose instrument for imaging and spectroscopy, with 0.58 arc-seconds/pixel and a FOV of 13x 12.6 arc-min.

The success of the determination of the main frequencies of the objects depends mostly on the accuracy of the measurements of the flash peaks. An automatic pipeline has been developed to process the data. In this paper, an accurate analysis of determining the end of the target streak ends is proposed to avoid systematic error in frequency analysis of the variability of the GEO objects.

1 INTRODUCTION

Observation of space debris are used to fit computer models to predict future growth of the debris population, and thus the probability of collisions with satellites, under different expectations. To model the orbital debris environment, it is necessary to collect data regarding actual situation, thus optical measurements are required. The Inter-Agency Space Debris Coordination Committee (IADC) [1] has promoted international observation campaigns for debris determination in different orbital regimes. The aim is to determine and characterize the space debris at different orbital regimes. For higher orbit, such as GEO (Geosynchronous Earth Orbit), only optical observation data can characterize space debris and provide an actual support for orbit determination and close approach analysis for collision avoidance manoeuver [2-4].

Recent break-ups events, the increase in small satellite cluster launches (i.e. CubeSat), the consequential increasing of the risk of collisions after the deployment [5], encourage to further improve their capabilities in space debris environment surveillance.

Since 2001 an extensive series of observations of the GEO regime has been carried out with University of Michigan's 0.6m Curtis-Schmidt telescope located at Cerro Tololo Inter-American Observatory in Chile (CTIO) revealing a considerable population of objects smaller than 1 m in diameter [6] to determine the total population of debris objects at GEO to as small a limiting size as possible.

Moreover, an Italian pilot program for the physical characterization of the space debris population in high Earth orbit was started in 2011 at the 152cm G.D. Cassini Telescope in Loiano, operated by the INAF Astronomical Observatory of Bologna, Italy [7- 10].

In 2014 a joint project among Astronomy Department of University of Michigan and S5Lab of Sapienza – University of Rome has started to study and analyze light-curve as indicator of the dynamic state of orbiting debris [11-12]. Generally, active satellites at GEO are typically attitude controlled. This control ceases in the case of loss of control, or when the satellite is moved to a graveyard orbit and then decommissioned. The idea of the on-going project is to investigate how rapid changes in brightness of the debris can imply rapid

Proc. 7th European Conference on Space Debris, Darmstadt, Germany, 18–21 April 2017, published by the ESA Space Debris Office
Ed. T. Flohrer & F. Schmitz, (http://spacedebris2017.sdo.esoc.esa.int, June 2017)

changes in attitude. To perform this analysis an automatic pipeline code has been developed and tested on observations taken while the telescope is tracking at the sidereal rate, and the GEO object is trailed across the field of view (FOV). The data have been acquired at the Curtis-Schmidt at CTIO and the Loiano Observatory. Analysis of intensity changes along the trail reveals the primary frequencies of the object's brightness variations on time scales of a second or less.

Section 2 present the observatories used to collect data and the observing strategy, while Section 3 will present the description of the implemented algorithm for the analysis. The code has been tested on real data and the results are presented on Section 4 and the conclusions are given in Section 5.

2 OBSERVATORIES USED

These observations were performed using two telescopes:

- The Curtis-Schmidt telescope (Figure 1) is a 0.61-meter aperture f/3.5 Schmidt telescope located at the Cerro Tololo Inter-American Observatory (CTIO), about 500 km north of Santiago, Chile. The acronym for the orbital debris project is MODEST (Michigan Orbital DEbris Survey Telescope). The telescope is equipped with a single E2V thinned, backside illuminated CCD with 1.45 arc-seconds/pixel and a field of view of 1.6x1.6 degrees [6].
- The Cassini observatory (Figure 1), located at Loiano near Bologna at an elevation of 785 m. The average measured seeing all year around is about 2 arc-seconds (FWHM). The telescope is a 152cm diameter Ritchey–Chrétien configuration, system with f/3 at the primary. focus and f/8 at the secondary [13].

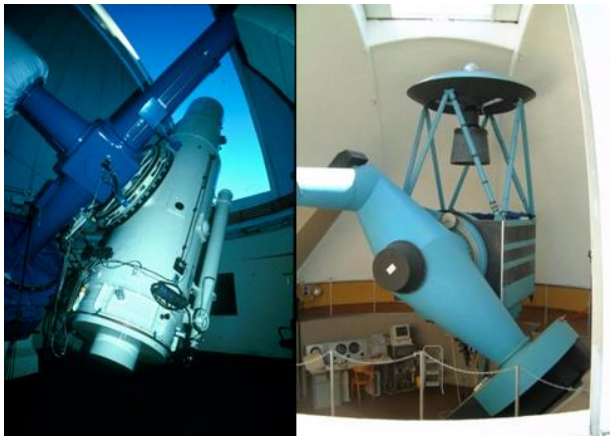

Figure 1. Curtis-Schmidt telescope at CTIO (left) and Cassini Telescope at Loiano Observatory (right).

Observations of a GEO target are typically sensitive to changes in brightness on timescales of 30 s or longer [12] primarily because of the long readout time (25 s) of the CCD. To investigate brightness changes faster than this, a different technique has been used. The object trailed across the field of view while the telescope tracked at the sidereal rate. R filter was used ([3], [12]). Exposure times were 20 s or longer, such that both ends of the trail were in the field of view. With image quality ("seeing") of approximately 2 arc-seconds FWHM, and the object moving at an average rate of 15.041 arc-seconds/s along track, the analysis will be sensitive to brightness variations as fast as 0.13 s. This is a factor of more than 100 times faster than variability detected in the standard satellite tracked observations reported above.

3 ALGORITHM DESCRIPTION

The tool can be divided into three main parts.

The first process (Figure 2) is the preliminary data procedure. All the collected images are reduced using a custom IRAF routine for bias and flat field. Then, the processed images are used as an input for the automatic tool. Right ascension (RA), declination (DEC), field of view of the observatory (FOV) and observation date are extracted and processed for the analysis. The whole TLE (Two-Line Element Set) public catalogue for GEO objects is downloaded [14] at the specific tame of the observation. Therefore, all TLEs are propagated to calculate if their astronomical coordinates could be inside the specific FOV of each image. A list containing each image file name and the SSN (US Space Surveillance Network) identification code of the contained orbiting object is then created.

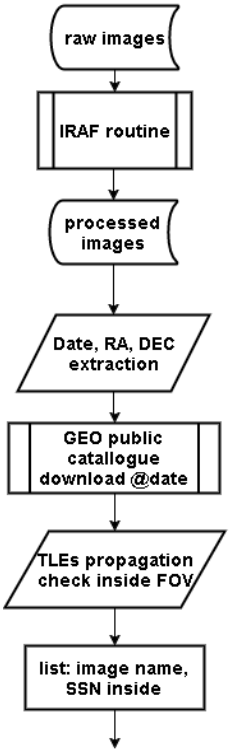

Figure 2. Preliminary data process flowchart.

The second part, presented in Figure 3, is the core for the streak identification process inside the image. The identification of the streak ends is crucial for the whole process of period determination from light-curves [15]. To reduce the effect of uncertainty of the observed streak ends, the TLEs of the observed targets have been used to determine theoretical length of the streaks by computing the rates. TLEs are released by United States Air Force periodically. An analysis on the variability of main orbit parameters have been performed to evaluate the effectiveness of the TLEs analysis at the observing period. The dataset of the identified objects over a period of twenty-day (plus and minus ten-day from the observing date) is automatically download and propagated individually to evaluate the predicted position of the target in the FOV of each image. This minimizes confusion when multiple target streaks are collected on the same image (Figure 4).

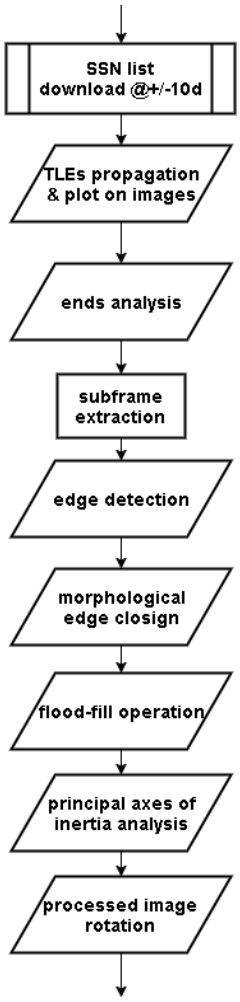

Figure 3. Streak extraction process flowchart.

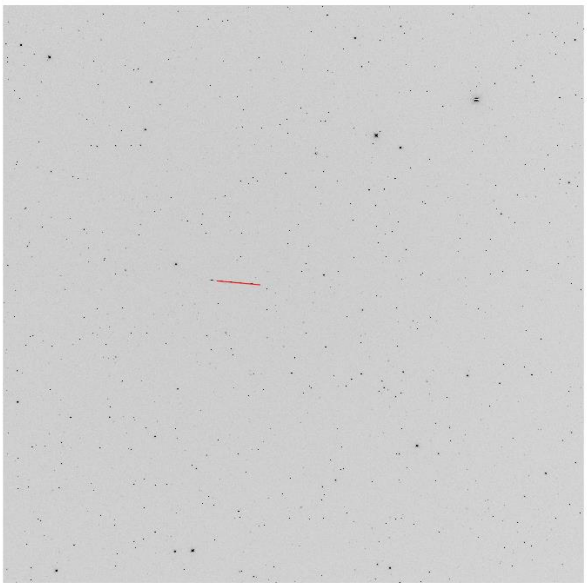

Figure 4. Original image with predicted streak obtained

from TLEs propagation over-impressed (red).

The median rates for both RA and DEC are evaluated by using all TLEs propagation. Therefore, the along-track rate is calculated as the norm of the two. By using the projected pixel dimension each observatory (1.45 arc-sec/pixel for MODEST [6] and 0.58 arc-sec/pixel [13]) the total streak length along-track for each TLE is computed. Therefore, the streak is extracted from the image as a sub-frame (Figure 5).

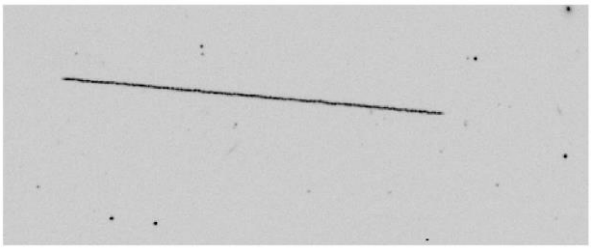

Figure 5. Streak sub-frame obtained from TLE propagation.

The automatic code applies an edge detection routine based on Canny algorithm [16]. The threshold values are chosen though an analysis of the image histogram with logarithmic scale. Then a morphological edge closing algorithm [17] is performed to return an edge-closed binary image (Figure 6) with filled holes [18] (Figure 7).

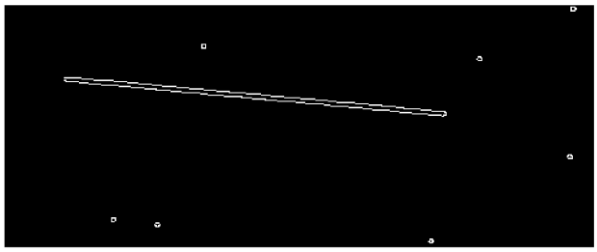

Figure 6. Edge detection results using Canny algorithm.

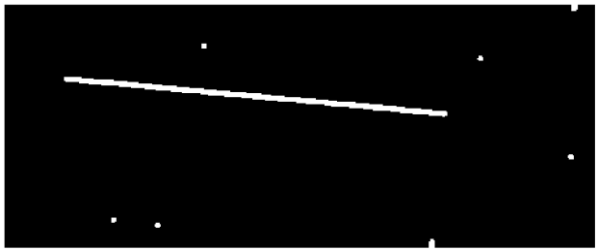

Figure 7. Binary image with edge-closed and filled holes.

The binary sub-frame is then processed using a two-steps connected-component analysis to identify the targets in the field. The major and minor axis expressed in pixel of each connected-component are evaluated. These values are the length of the major, or minor, axis of the ellipse that has the same normalized second central moments as the identified region [4]. As described in Paragraph 2, all images are obtained by moving the telescope at sidereal rates. Consequently, the stars appear as circle while the object trails across the FOV as a streak. The algorithm identifies stars as the objects with major-minor axis ratio close to one. On the contrary, the streaks will have a ratio greater than one, function of several parameters such as the exposure time, the "seeing" (FWHM), trailing rates and the sensor's characteristics. For example, by considering an exposing time equal to 20 seconds, an average trailing rate of 15.041 arcsec/sec (equal to sidereal rate), a pixel-scale equal to 1.45 arcsec/pixel, the seeing of about 2 arcsec, it is possible to have an aspect ratio value greater than 50. A safety factor equal to five is then applied. Therefore, the orbiting objects are identified as the connected object which major-minor axes ratio exceeds 10 (Figure 8).

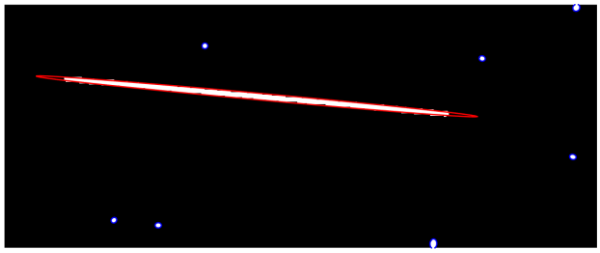

Figure 8. The connected objects are identified: stars are shown in blue while the object streak is marked in red.

Once the target in the binary sub-frame is identified, the centroid coordinates and the streak orientation θ are evaluated. The centroid is computed as center of mass of the connected-object. Its coordinates in the sub-frame reference system are then converted the main frame reference system. The frame is then rotated of the same orientation angle θ.

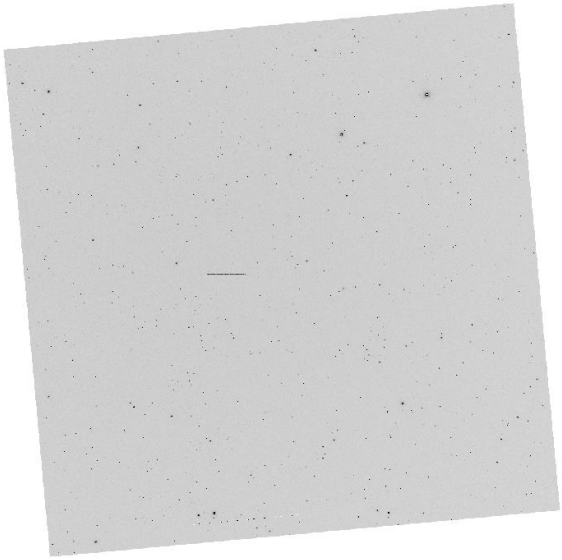

Figure 9. Image rotated by θ.

The third part of the code is summarized in Figure 10. Its main feature is to extract the tumbling period of the streaked object from the light-curves.

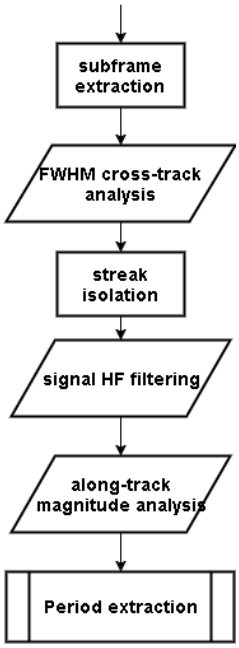

Figure 10. Streak analysis process flowchart.

The rotated image from the previous step is analyzed to extract the sub-frame that contain the horizontal streak. The streak ends on the rotated image are evaluated by considering the median value of the predicted streaks length computed from the TLEs and a sub-frame is extracted. The code performs a cross-track analysis on the sub-frame to evaluate the instantaneous seeing of the streak during the exposition. The object radius value is evaluated as half the size of the cross-track dimension that contains at least 3σ, where σ is the standard deviation of the counts values in cross-track direction (Figure 11). The streak signal is isolated from the sub-frame and then analyzed.

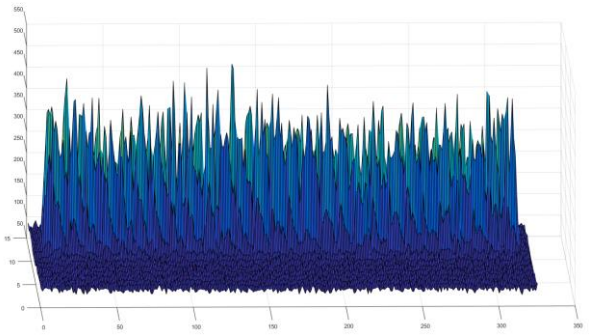

Figure 11. Three-dimensional representation of the streak.

A seeing analysis is performed to evaluate the streak length. The total counts in cross-track direction are summed and the median value of sky level is then subtracted. The ends of the streak are then evaluated as the ends point along track where the total counts are above sky level. Generally, orbiting object do not have a constant brightness. They reflect flashes at typically regular times that are caused by their tumbling motion. The specular reflection of the satellite's metallic surfaces that act as mirrors for the sun causes flashes brighter than the diffuse reflection from the other part of the body that can be dimmer than sky background. Therefore, the optical signatures could appear as a series of disconnected round flashed when observed on CCD images. Per Somers [15], when the flash occurs near the beginning or end of the time exposure, the location of the end is obscured, and strategy to accurately assign an accurate time scale to the streak are needed.

The solution implemented in the algorithm consist in a comparison between the calculated and the predicted median streak length. If the length evaluated from the image is less than the one evaluated by the TLEs, the difference in pixels is added to the ends. The error in the ends detection could occur in both extremes or just in one of the two ends. The code applies a streak-ends shifting technique to produce image light-curves with the same length as the predicted ones. If for example (Figure 12), if the original length is shorter than the one computed from the rates of the TLE by 2 pixels, all combinations (difference in pixels +1 = 3) are calculated by shifting the ends of one pixel at the time to have all the same lengths as the one computed from the TLE.

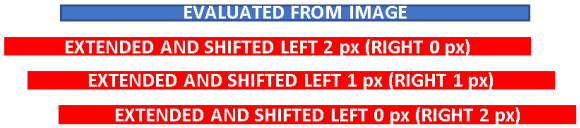

Figure 12. Shift process example.

All obtained streaks are analyzed separately and a Savitzky–Golay filter [19] is then applied to smooth noisy data at high frequency. The implemented low-pass filter is based on local least-squares polynomial approximation of the fourth order. Therefore, the instantaneous magnitude in the along-track direction evaluated (Figure 13).

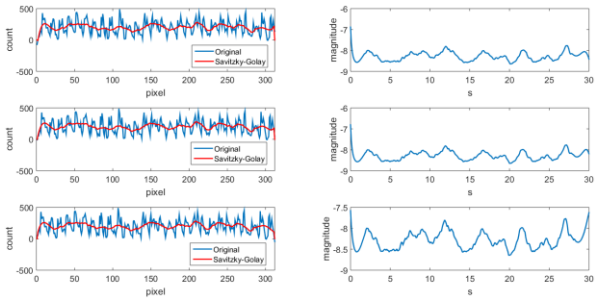

Figure 13. Count (on the left) and calibrated magnitude (on the right) plots for each light-curve obtained by the shifting process.

To extract the flashing period three algorithms are implemented [20]. The first one uses Fast Fourier Transformation (FFT) [21] to evaluate the main frequencies. The second one uses Periodogram power spectral density (PSD) estimation [22], while the third Lomb-Scargle power spectral density [23] estimation where the sampling frequency fs is estimated as the along-track streak length (expressed in pixel) divided by the exposing time (expressed in seconds). FFT is commonly used to extract frequencies from light-curves (20). Therefore, the Periodogram analysis and Lomb-Scargle method were chosen to be validated with FFT.

4 RESULTS

The as test case the automatic pipeline has been applied to the observation taken at MODEST (Table 1) and at Loiano Observatory (Table 2).

Table 1. Number of trailed images taken at MODEST on November 3, 2015.

SSN	LAUNCH YEAR	NUMBER OF TRAILED IMAGES
13056	1982	9
19217	1988	8
23536	1995	6
23846	1996	8
25152	1998	7

Table 2. Number of trailed images taken at the Loiano Observatory on February 10, 2016.

SSN	LAUNCH YEAR	NUMBER OF TRAILED IMAGES
17873	1979	1
18718	1987	3
27509	2002	2
27780	2003	3

The results of the main frequencies expressed in Hz, extracted with the three methods (FFT, Periodogram and Lomb-Scale) are presented in Table 3 and Table 4.

Table 3. Main four frequencies (in Hz) detected from MODEST data with the highest power (in dB). The symbol "--" represents that the specific frequencies was not identified by the methods among the first four frequencies with the highest power.

SSN	FFT	Periodogram	Lomb-Scargle
13056	--	0,02	0,023
	0,067	0,06	0,067
	--	0,1	0,108
	0,202	0,201	0,2
	0,263	--	--
	0,679	--	--
19217	0,071	0,07	0,077
	0,131	0,12	0,133
	0,263	0,2595	0,258
	0,403	0,405	0,404
23536	--	0,02	0,025
	0,131	0,131	0,135
	0,202	--	--
	0,3	0,302	0,3
	0,465	0,463	0,462
23846	--	--	0,029
	0,071	0,071	0,067
	0,101	0,104	0,108
	0,303	0,305	0,306
	0,737	0,739	--
25152	--	0,07	0,075
	--	--	0,168
	0,202	0,221	0,221
	0,303	0,301	0,308
	0,364	0,441	--
	0,505	--	--

Table 4. Main four frequencies (in Hz) detected from Loiano data with the highest power (in dB). The symbol "--" represents that the specific frequencies was not identified by the methods among the first four frequencies with the highest power.

SSN	FFT	Periodogram	Lomb-Scargle
17873	--	0,052	0,05
	0,2	0,193	0,195
	0,354	0,363	0,358
	0,505	--	--

	0,646	0,642	0,658
18718	0,101	0,107	0,104
	0,202	0,2	0,2
	0,303	--	--
	0,505	0,5605	0,55
	--	1,014	1,013
27509	0,101	0,109	0,108
	0,152	0,158	0,154
	0,253	--	--
	0,354	0,351	0,355
	--	0,799	0,75
27780	0,151	0,154	0,162
	--	0,231	0,237
	0,303	0,308	0,3
	0,505	--	--
	0,596	0,59	0,6

Due to the observing strategy, the automatic pipeline is capable to identify frequencies within a range that depends on the exposure time and the pixel scale of each observatory used. In particular, the minimum detectable frequencies is 1/Texp = 1/30sec = 0.033 Hz, while the maximum detectable frequencies is 1/(trailing rate/pixel scale) = 10Hz for MODEST data and 25Hz for Loiano data.

The presented results show the consistency of the three methods. The first four frequencies with the highest power have been identifies and the results are homogenous. It is possible to notice that the frequencies obtained from both observed target with MODEST and Loiano telescope are mainly distributed in the range between 0.1 and 0.5 Hz (Figure 14 and Figure 15).

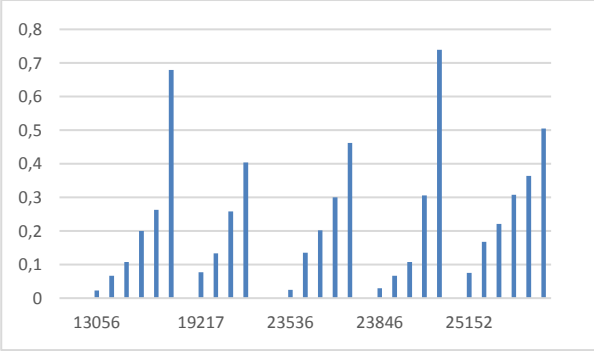

Figure 14. Histogram of the main frequencies (in Hz) detected from MODEST data.

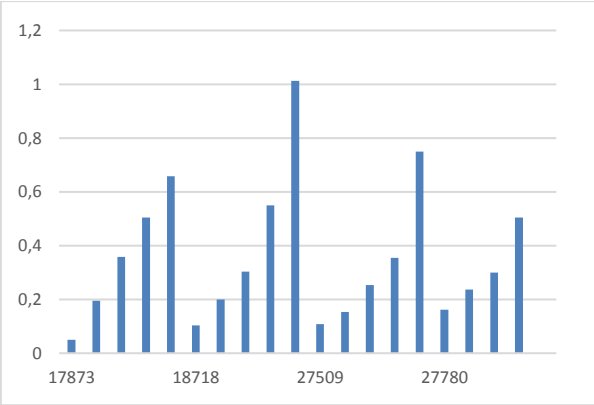

Figure 15. Histogram of the main frequencies (in Hz) detected from Loiano data.

5 CONCLUSIONS

The development of an automatic pipeline for light-curve extraction for frequencies analysis of GEO objects has been presented. Light-curves analysis proved to be an effective method to determine the attitude of orbiting objects including space debris. The presented paper outlines the main phases of the streak identification process, with a special focus on how to solve the problem on determination of streaks ends. Possible application of this technique might include streaks detection on mosaic CCD when the trail passes across the gap or the ends occurs within the gap.

The presented code has been tested on images collected from MODEST at CTIO in Chile and from Cassini Observatory in Italy. The observations have been collected with the object trailed across the field of view while the telescope tracked at the sidereal rate. More observations of space debris as streaked images are necessary to improve the knowledge of the main frequencies of the objects, and to determine how the evolution of the dynamic state of the orbiting object with time.

Different methods for the main frequencies determination of the attitude from the streaked light-curves have been developed.

6 ACKNOLOGEMENTS

The research work presented in this paper is supported by the Italian Space Agency, in the framework of the ASI-INAF Agreement “Supporto alle attività lADC e validazione pre-operativa per SST” (N.2015-028-R.0).

The authors wish to acknowledge support from the University of Michigan Department of Astronomy for MODEST operations. Moreover, the authors would like to thank for support received from the staff and technicians of the Loiano Observatory for their invaluable help during the observing sessions.

7 REFERENCES

1. IADC Space Debris Mitigation Guidelines, (2002).
2. Piergentili, F., Ravaglia, R., Santoni, F., “Close approach analysis in the geosynchronous region using optical measurements”, Journal of Guidance, Control, and Dynamics, Volume 37, Issue 2, pp. 705-710 (2014).
3. Santoni, F., Cordelli, E., Piergentili, F., “Determination of disposed-upper-stage attitude motion by ground-based optical observations”, Journal of Spacecraft and Rockets, Volume 50, Issue 3, pp. 701-708 (2013).
4. Piergentili, F., Ceruti, A., Rizzitelli, F., Cardona, T., Battagliere, M.L., Santoni, F., “Space debris measurement using joint mid-latitude and equatorial optical observations”, IEEE Transactions on Aerospace and Electronic Systems, Volume 50, Issue 1, pp. 664-675 (2014).
5. Santoni, F., Piergentili, F., Ravaglia, R. “Nanosatellite cluster launch collision analysis” Journal of Aerospace Engineering, Volume 26, pp. 618-627 (2013).
6. P Seitzer, P., Smith, R., Africano, J., Jorgensen, K., Stansbery, E., Monet, D., “MODEST observations of space debris at geosynchronous orbit”, Advances in Space Research, Volume 34, Issue 5, pp. 1139-1142 (2004).
7. Rossi, A., Marinoni, S., Cardona, T., Dotto, E., Perna, D., Santoni, F., Piergentili, F., “Physical characterization of space debris in the geosynchronous region” 62nd IAC - International Astronautical Congress (2011).
8. Rossi, A., Marinoni, S., Cardona, T., Dotto, E., Perna, D., Santoni, F., Piergentili, F., “The Loiano campaigns for photometry and spectroscopy of geosynchronous objects”, 63rd IAC - International Astronautical Conference (2012).
9. Rossi, A., Marinoni, S., Cardona, T., Dotto, E., Perna, D., Santoni, F., Piergentili, F., “Physical characterization of objects in the GEO region with the Loiano 1.5 m telescope”, 6th European Conference on Space Debris ESA/ESOC (2013).
10. Cardona, T., Seitzer, P., Rossi, A., Piergentili, F., Santoni, F., “Photometric characterization of GEO objects from the Loiano telescope”, 66th IAC - International Astronautical Congress (2015).
11. Piergentili, F., Santoni, F., Seitzer, P., “Attitude Determination of Orbiting Objects from Lightcurve Measurements”, IEEE Transactions on Aerospace and Electronic Systems, Volume: PP Issue: 99, 10.1109/TAES.2017.2649240 (2017)
12. Cardona, T., Seitzer, P., Rossi, A., Piergentili, F., Santoni, F., “BVRI photometric observations and light-curve analysis of GEO objects”, Advances in Space Research, Volume 58, Issue 4, pp. 514–527 (2016).
13. Gualandi, R., Merighi, R., “BFOSC – Bologna Faint Object Spectrograph & Camera - User Manual Technical Report. Version 2.0 (2001).
14. https://www.space-track.org, Retrieved March 30, 2017.
15. Somers, P., “Cylindrical RSO Signatures, Spin Axis Orientation and Rotation Period Determination”, AMOS - Advanced Maui Optical and Space Surveillance Technologies Conference (2011).
16. Canny, J., “A Computational Approach to Edge Detection”, IEEE Trans. Pattern Analysis and Machine Intelligence, 8(6):679–698, (1986).
17. Gonzalez, R., Woods, R. “Digital Image Processing”, Addison-Wesley Publishing Company, pp 524, 552, (1992).
18. Soille, P., “Morphological Image Analysis: Principles and Applications”, Springer-Verlag, pp. 173-174, (1999).
19. Savitzky, A., Golay, M., “Smoothing and differentiation of data by simplified least squares procedures”, Anal. Chem. (1964).
20. Schildknecht, T., Linder, E., Silha, J., Hager, M., Koshkin, N., Korobeinikova, E., Melikiants, S., Shakun, L., Strakhov, S., “Photometric Monitoring of Non-Resolved Space Debris and Databases of Optical Light Curves”, AMOS - Advanced Maui Optical and Space Surveillance Technologies Conference (2015).
21. Welch, P. D., The Use of Fast Fourier Transform for the Estimation of Power Spectra: A Method Based on Time Averaging Over Short, Modied Periodograms," IEEE Transactions on Audio and Electroacoustics, Vol. AU-15, No.2, JUNE 1967, (1967).
22. http://ch.mathworks.com/help/signal/ref/periodogram.html, Retrieved March 30, 2017.
23. https://it.mathworks.com/help/signal/ref/plomb.html, Retrieved March 30, 2017.

.